JOURNAL OF APPLIED ELECTROCHEMISTRY 25 (1995) 923–932

Hydrogen evolution reaction on electrocatalytic materials highly dispersed on carbon powder

J. FOURNIER, H. MÉNARD

Département de Chimie, Université de Sherbrooke, Sherbrooke, Québec, Canada J1K 2R1

L. BROSSARD

Institut de Recherche d'Hydro-Québec (IREQ), 1800 montée Ste-Julie, Varennes, Québec, Canada J3X 1S1

Received 5 October 1994; revised 2 March 1995

Highly dispersed electrocatalytic materials were obtained by vacuum deposition of catalytic metals on electromechanically suspended graphite powder particles. Graphite electrodes, vacuum-deposited with various metals (Ni, Pt, Au, Pd, Rh) or an alloy (Cu–Al), were bonded with an inorganic polymer, $LaPO_4$. A.c. impedance and steady-state polarization methods were used to investigate the mechanism and kinetics of the hydrogen evolution reaction (HER) in 1 M KOH at 25 °C for Pt/C, Pd/C and Rh/C electrodes. It was concluded that the HER follows a Volmer–Heyrovsky mechanism.

1. Introduction

The hydrogen evolution reaction (HER) has been extensively investigated in the literature [1–5]. This reaction may be schematically described as composed of three elementary steps:

Volmer reaction

$$H_2O + M + e^- = MH_{ads} + OH^- \qquad k_1, k_{-1} \qquad (1)$$

Heyrovsky reaction

$$H_2O + MH_{ads} + e^- = M + H_2 + OH^- \qquad k_2, k_{-2} \qquad (2)$$

Tafel reaction

$$2MH_{ads} = 2M + H_2 \qquad k_3, k_{-3} \qquad (3)$$

where indicated k_S represent the respective rate constants of the forward (+) and backward (−) processes. Water reduction with hydrogen adsorption (Reaction 1) is followed by electrochemical (Reaction 2) and/or chemical (Reaction 3) desorption. The rates (v) of these processes are described by the equations

$$v_1 = k_1(1-\theta)\exp(-\alpha_1 f\eta) - k_{-1}\theta\exp[(1-\alpha_1)f\eta] \quad (4)$$

$$v_2 = k_2\theta\exp(-\alpha_2 f\eta) - k_{-2}(1-\theta)\exp[(1-\alpha_2)f\eta] \quad (5)$$

$$v_3 = k_3\theta^2 - k_{-3}(1-\theta)^2 \quad (6)$$

where α denotes the transfer coefficient, θ the surface coverage of the electrode by adsorbed hydrogen, and $f = F/RT$.

Early studies by Bockris, Conway and Parsons [6] showed that the rate constants of the HER reach a maximum with the platinum group metals, but that cheaper nickel-based electrodes are also very active electrocatalysts. For hydrogen evolution in alkaline media [7–9], the Ni-based electrode can be made by various methods such as sintering, vacuum or plasma-sprayed deposition, electrodeposition or high-temperature deposition [7, 10–16]. High surface area nickel electrodes are also obtained using a tridimensional inorganic polymer of aluminium or lanthanum phosphate ($AlPO_4$ or $LaPO_4$), which cements the metallic particles [17–20]. These electrodes are more stable in aqueous alkaline solution when made with $LaPO_4$ rather than $AlPO_4$, because it is less soluble in such solutions [20]. This new process is particularly attractive because cementation can be achieved without a reducing atmosphere (only the presence of inert gas is required).

Very active metallic powders such as platinum should not normally be used, since they are expensive compared to nickel, but they may be more attractive for the HER or other electrochemical processes if they are well dispersed by vacuum deposition on a graphite powder.

Graphites have been widely used as electrode materials in the chlor-alkali industry. Besides being relatively inert chemically in most electrolytes, carbon can be obtained as high-surface-area powders as well as in solid-electrode form. For the preparation of high surface area electrocatalysts, carbon offers many attractive properties, namely chemical stability, high surface area, good electrical conductivity and favourable (macroscopic and microscopic) porosity.

Vacuum deposition of catalytic metals on a solid graphite substrate has been known for a long time, whereas successful vacuum deposition on graphite powder is very recent [21]. The process consists in applying catalytic metals (Ni, Rh, Pt, Pd, ...) or alloy (Al–Cu) under vacuum on an electromechanically suspended graphite powder. Deposition of catalytic material is performed by heating a powder or wire of the metal (or alloy) concerned on a refractory

0021-891X

support material under vacuum (10^{-5}–10^{-6} mbar). The graphite powder (substrate) is fluidized by shaking it over a surface vibrating at low frequency (~ 200 Hz).

Since graphite is very loosely bonded, paste electrodes of the Adams type [22], in which various hydrocarbons are used as binding substances, would tend to disintegrate under a large flow of hydrogen when graphite is used as the cathode for alkaline water electrolysis. In our laboratory, graphite powder electrodes were therefore made with lanthanum phosphate as the binding material, which yielded strongly bonded graphite particles.

In the present study, the electrochemical behaviour of graphite powder vacuum-deposited with various metals and bonded by $LaPO_4$ polymer was investigated for the HER in a 1 M KOH solution at 25 °C. The electrodes with vacuum-deposited rhodium (2.1 wt %) had a hydrogen overvoltage as low as −168 mV for $j = 0.10\,A\,cm^{-2}$ (1 M KOH at 25 °C), that is, much lower than for electrodes prepared with a nickel powder. HER investigation of vacuum-deposited highly dispersed electrocatalytic materials is a further step in an ongoing evaluation of their potential application in electrohydrogenation processes.

2. Experimental details

2.1. *Preparation of catalytic powders*

Natural graphite powder (Superior Co.) was used as the substrate for vacuum deposition of the catalytic metals. The graphite was heated overnight at 250 °C under an argon flow to remove water and some of the species adsorbed on the surface before introducing it in the evaporation system.

A diagram of the vacuum deposition setup is given in Fig. 1. The apparatus comprises a glass evaporation chamber (2) with a ~ 30 cm diameter which is filled through a loading port (3). Vacuum (on the order of 10^{-5}–10^{-6} mbar) is obtained by a pumping system comprising a water cooled (6) oil diffusion pump (4). This pump is connected to the evaporation chamber by an oil baffle (7) filled with liquid nitrogen (8) and a pneumatic valve (9) which allows the pump to be kept under vacuum and at the operating temperature even when the chamber is at atmospheric pressure. Prior to connection to the diffusion pump in the purpose of realize high vacuum, the chamber must be evacuated by means of a rotary mechanical pump (10) by opening valve (9). The rotary pump is connected to the system itself by two other valves, the first (11) to the evaporation chamber and the second (12) to the back of the diffusion pump. A gas admittance valve (13) is located at the gas input. A Pirani gauge (14) is used for measuring the gas pressure during mechanical pumping and detecting leak. A Penning cold-cathode type of ionization gauge (15) is used for the very low pressure measurements, low-pressure values being a key factor for favourable coating conditions.

A 3000 VA transformer (16) ensures the evaporation of catalytic metals by resistance heating of refractory metal (W, Mo, Ta) heaters in the form of filaments or inverted boats (17). Three filaments or inverted boats can be heated either in succession or simultaneously in the apparatus described. For long evaporation times, a cooling system (18) serves to reduce heat-generated stress in the evaporation chamber. The substrate powder is placed in an aluminium boat (19) which is maintained on the audiofed surface (20) by four small springs (21). An amplifier (22) feeds the output from a sinusoidal signal generator (23) to the vibrating surface. Surprisingly, it proved possible to obtain powder in the shape of a fluidized bed over a vibrating surface without resorting to gas circulation through the bed. Depending on the density of the powder to be fluidized, the frequency was adjusted manually to obtain good dispersion over this surface to take into account variations in the density of the substrate powder. Since the fluidizing frequency of the powder substrate is also linked to the pressure, it was continuously adjusted during metal evaporation to take into account increases in the pressure in the evaporation chamber throughout this process.

2.2. *Preparation of the electrodes*

The $M/C/LaPO_4$ electrodes were prepared with graphite powder containing various amounts of a deposited metal: Ni, Pt, Cu, Pd and Rh. Lanthanum phosphate was prepared by combining acid lanthanum phosphate and lanthanum hydroxide [23]. Two reactions are involved in the formation of acid phosphate lanthanum $La(H_2PO_4)_3$ and its subsequent transformation into $LaPO_4$

$$1/2\,La_2O_3 + 3H_3PO_4 \longrightarrow La(H_2PO_4)_3 + 3/2\,H_2O \quad (7)$$

$$La(H_2PO_4)_3 + 2La(OH)_3 \longrightarrow 3LaPO_4 + 6H_2O \quad (8)$$

$La(H_2PO_4)_3$ was synthesized by adding 48.88 g (0.15 mol) La_2O_3 to 103.7 g (0.90 mol) H_3PO_4 (85%) in a rectangular Teflon cell, 10 cm × 5 cm × 5 cm (Teflon was used rather than a reactive intermediate which may react with glass).

The reaction product, in the form of a viscous paste, was heated in an oven at 150 °C for 24 h and vacuum-dried to remove traces of water generated by the reaction. Powders of $La(H_2PO_4)_3$ and $La(OH)_3$ were mixed thoroughly with a graphite powder (with or without a metal deposit) in a 1 : 1 ratio. Approximately 1 g of the resulting powder was pressed at 7040 kg cm^{-2} under vacuum in a mould with a diameter of 1.28 cm^2. A nickel foil was inserted into the pellet to obtain a good electrical contact.

The polymerization reaction was carried out under argon by heating the pellets for 8 h at 400 °C, after which one side was coated with Epofix resin (Struers). The exposed surface area of the electrode was 1.29 cm^2.

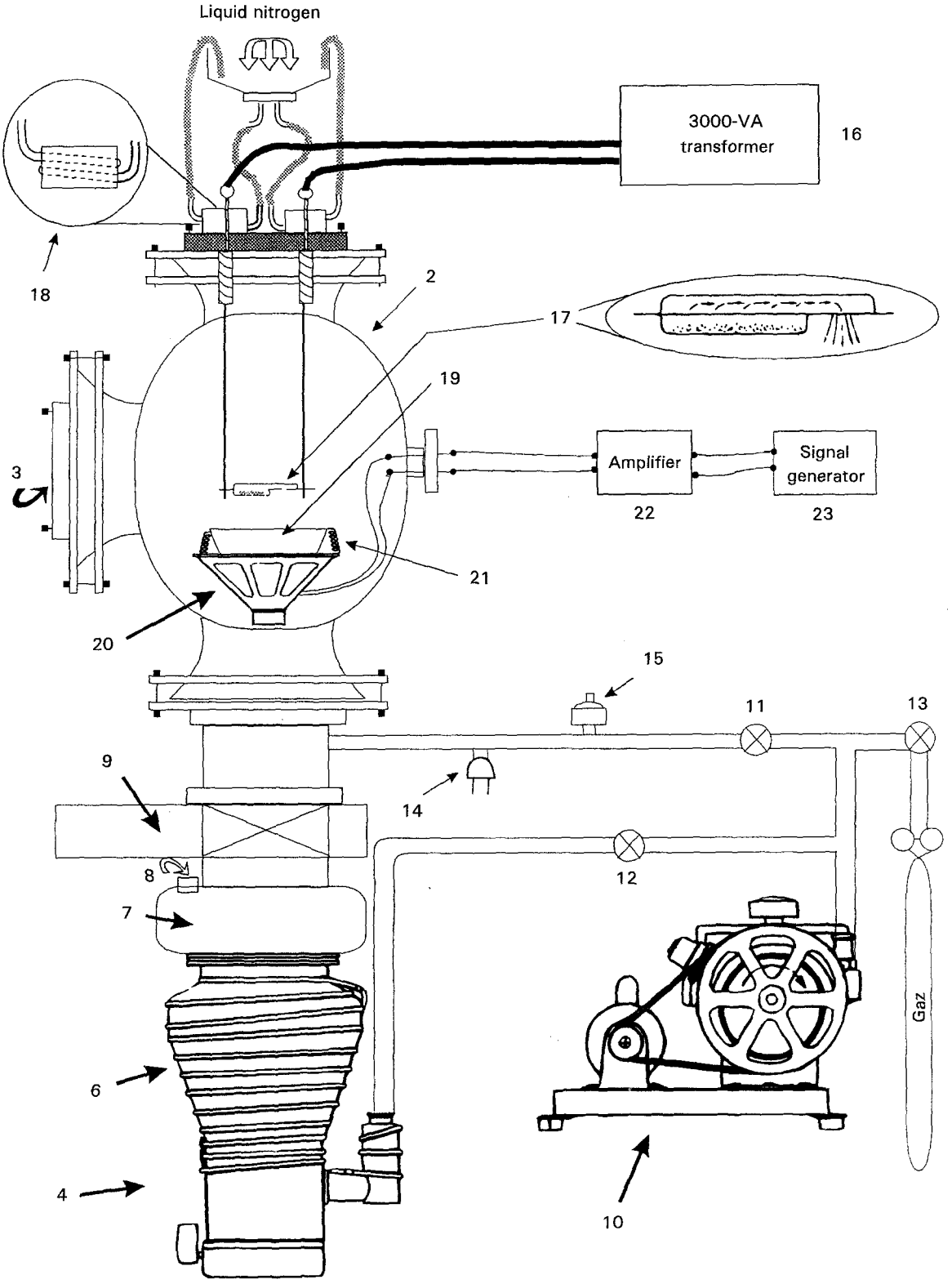

Fig. 1. Apparatus for preparation of highly dispersed catalytic materials.

The nature of the solid polymer resulting from Equation 8 was previously determined (by XRD) to be a three-dimensional polymer $LaPO_4$ [24], the crystallographic parameters of $LaPO_4$ being similar to those reported for monazite [25, 26].

2.3. *Data acquisition*

The Tafel plots were established using an EG&G (model 273) potentiostat. The same potentiostat and an EG&G 5208 lock-in analyser were used for the impedance measurements. The experiments were controlled by an IBM-compatible microcomputer.

All the experiments were carried out in a 1 M KOH (BDH Aristar) solution using deionized water (Barnstead Nano-pure) and the solution was deaerated by bubbling nitrogen through it.

The electrochemical cell was made of Pyrex and the anodic compartment was separated by a Nafion® membrane M-901CATH/MD (duPont).

A Luggin capillary was used to minimize the ohmic drop.

The reference electrode was a Hg/HgO electrode in 1 M KOH kept at room temperature. The counter electrode was a high surface area nickel grid.

3. Results and discussion

3.1. *Characteristics of the deposits*

The yield values of the metal deposition are summarized in Table 1 for the different metals or the alloy studied. The yield is the ratio between the amount of metal or alloy deposited on graphite powder and the amount of metal or alloy contained in the vessel (made of refractory material) prior to evaporation. The evaporation process was carried out in such a way that all the metal or alloy contained in the vessel was evaporated. The refractory materials, the evaporation time and the temperature [27, 28] are given in Table 1 but in many cases rapid evaporation started at temperatures well above those in the Table 1 because of a surface oxide film on metals to be evaporated.

The structure of the graphite powder in the presence or absence of a metal deposit was investigated by transmission electron microscopy (TEM). The TEM picture in Fig. 2 clearly shows that these particles have a lamellar structure (average diameter of 50 μm). Figure 3 illustrates a nickel deposit (10 wt %) on a graphite particle. This deposit has a fine cluster structure (< 1 μm) and a relatively uniform distribution over the entire surface. It should be noted that because electrons pass through the particles, the deposit appearing in the TEM picture corresponds to the simultaneous projection of the two faces of a particle. For a larger amount of nickel coating, i.e. 20 wt %, the deposit is nodular (Fig. 4) with a larger particle size compared to that for 10 wt % Ni (Fig. 3). Another example is given for a 5.4 wt % platinum deposit on a graphite particle (Fig. 5) which shows a uniform dispersion of metal on a graphite particle surface.

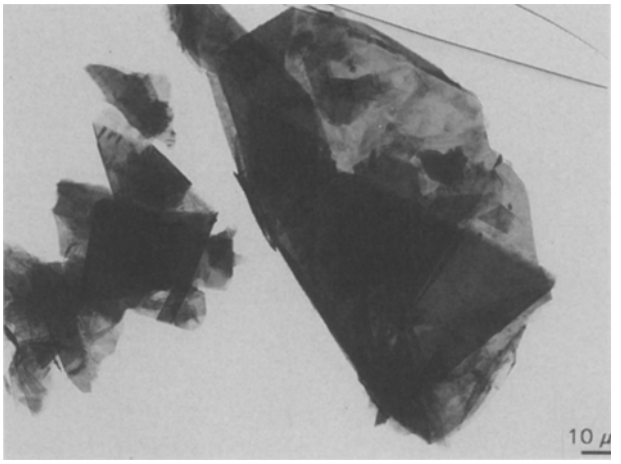

Fig. 2. Graphite particle (Superior Co) seen by TEM (X10000).

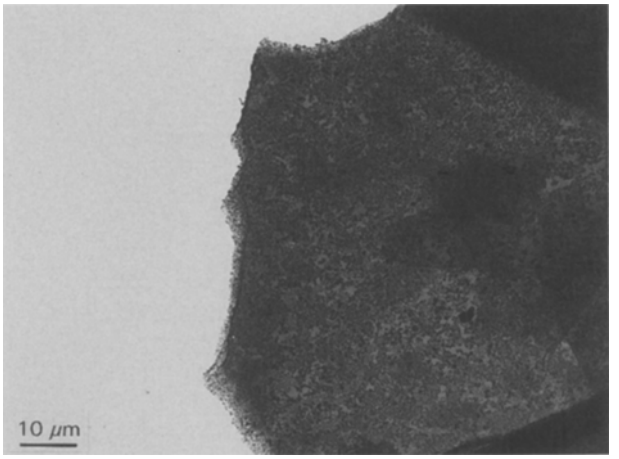

Fig. 3. Ni/C (10 wt %) particle seen by TEM (X16000).

For a natural carbon powder, the specific surface area is 6.05 $m^2 g^{-1}$ and 7.212 $m^2 g^{-1}$ without nickel and with 10 wt % nickel, respectively (Table 2). It is deduced that the small asperities induced by the presence of a deposit favour the increase of the specific surface area up to approximately 15 wt % nickel. For a larger amount of metal deposit, i.e. 20 wt % or more,

Table 1. Deposition conditions and yields

Metals deposited on carbon powder	*Evaporation temperature* (v.p. = 10μHg)* /° C	*Evaporation time* /min	*Refractory material for the evaporation of metals*	*Yield*† /%
Ni	1510	15	W (inverted boat)	53
Pt	2090	10	W (filament)	35
Cu–Al	1037	5	Mo (inverted boat)	89
Au	1465	5	W (filament)	58
Pd	1555	10	W (filament)	21
Rh	2149	8	W (filament)	35

* Refs. [24, 25].

† Ratio between the amount of metal or alloy deposited on graphite powder and the amount of metal or alloy present before complete evaporation in a vessel made of a refractory material.

Fig. 4. Ni/C (20 wt %) particle seen by TEM (X12500).

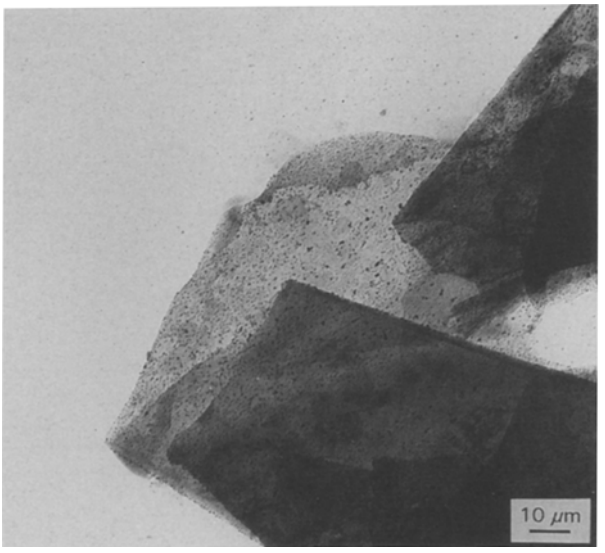

Fig. 5. Pt/C (5.39 wt %) particle seen by TEM (X10000).

the specific surface area decreases as the micropores are filled.

3.2. *Characteristics of M/C/LaPO$_4$ electrodes*

White spots of $LaPO_4$ binder on graphite (which is black) are noticed for a graphite electrode bonded with 50 wt % $LaPO_4$ (Fig. 6); the picture was obtained by SEM (Jeol JSM-840A) in a composition mode. The porosity and chemical stability of this material are both good [23]. The porosity of the electrodes

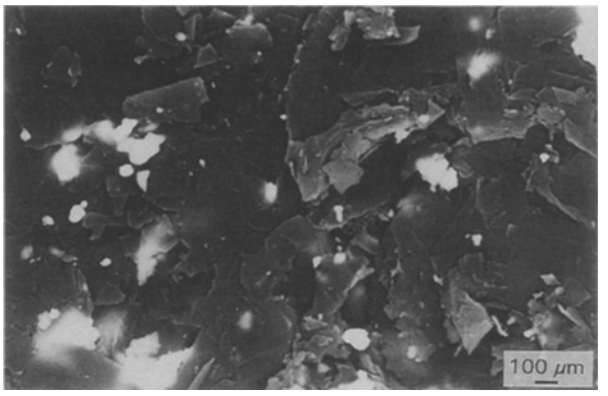

Fig. 6. C/$LaPO_4$ electrode surface (50 wt % $LaPO_4$) obtained by SEM (X700, 20 kV, WD18).

was determined by a mercury porosimeter (Carlo Erba ES 200). The volume of mercury intruded at a pressure of 150.1 MPa which was applied to force mercury into the pores was 35.2 $mm^3\ g^{-1}$. The chemical stability was determined by keeping the electrodes in a 30 wt % KOH solution (88 °C) at open-circuit potential and monitoring the weight for five consecutive days. The weight loss of less than 3 wt % was ascribed to the removal of unpolymerized $LaPO_4$.

In a different set of experiments, fresh electrodes made with a natural graphite powder and a graphite powder with a deposited metal were polarized under a cathodic current density of 0.1 A cm^{-2}. The increase in the hydrogen overvoltage was in the order of 20 mV after two days of polarization for all materials investigated, most likely due to the removal of unbonded metal on the graphite surface. The parameters of the hydrogen evolution reaction (HER) after two days of polarization are summarized in Tables 2 to 5.

Graphite electrodes free of deposited metal are characterised by a high hydrogen overvoltage at 0.1 A cm^{-2} (η_{100}) as shown in Table 2. It has been found for the Ni/C electrodes that the larger the specific surface area, the lower is η_{100}, as may be expected. The slight increase in η_{100} from 15 wt % to 20 wt % Ni is related to a somewhat smaller specific surface area.

For Cu–Al deposits, the aluminium was leached by reaction of deposit with 1 M KOH at 50 °C for 2 h prior to the polarization and the electrocatalytic activity is linked to the specific surface area (i.e., surface roughness factor) the latter being related to the amount

Table 2. Specific surface area and kinetic parameters of the HER on graphite powder with or without deposited Ni metal and bonded with 50 wt % of $LaPO_4$

Ni/C deposit /wt % ± 1 wt %	*BET** /$m^2\ g^{-1}$	*Overpotential*† at 0.1 A cm^{-2} /mV	*Exchange-current density*† /mA cm^{-2}
0‡	6.05	−525	0.010
10	7.21	−315	0.112
15	7.66	−311	0.188
20	7.62	−330	0.157

* Powder sample.
† After two days of polarization at 0.1 A cm^{-2} for the HER in 1 M KOH at 25 °C.
‡ Pure graphite powder.

Table 3. Specific surface area and kinetic parameters of the HER on graphite powder deposited with Cu–Al alloy and bonded with 50 wt % $LaPO_4$

Cu–Al/C deposit *Cu–Al 1 : 1* /wt % ± 1 wt %	*BET*† /$m^2\,g^{-1}$	*Overpotential*‡ *at 0.1 A* cm^{-2} /mV	*Exchange-current density*‡ /$mA\,cm^{-2}$
10	7.03	–	–
10 (after leaching)*	7.34	−468	0.03
15	6.72	–	–
15 (after leaching)*	9.96	−418	0.174

* Leaching of aluminium on powder (NaOH 1 M, 50 °C, 2 h).
† *Idem* Table 2.
‡ *Idem* Table 2.

Table 4. Kinetic parameters of the HER on graphite powder deposited with platinum metal and bonded with 50 wt % of $LaPO_4$

Pt/C deposit /wt % ± 0.09 wt %	*Overpotential*† *at 0.1 A* cm^{-2} /mV	*Exchange-current density*† /$mA\,cm^{-2}$	*Tafel slope*† /mV $(decade)^{-1}$
1.31	−388	2.31	234
2.45	−360	2.60	225
5.39	−320	0.79	151
50.0*	−333	3.26	223

* Mixed powder (Pt and graphite).
† *Idem* Table 2.

Table 5. Kinetic parameters of the HER on graphite powder deposited with various metals and bonded with 50 wt % $LaPO_4$

M/C deposit	*Overpotential* at 0.1 A* cm^{-2} /mV	*Exchange-current density** /$mA\,cm^{-2}$	*Tafel slope** /mV $(decade)^{-1}$
Au (36 ± 5 wt %)	−498	0.89	241
Pd (0.2 ± 0.1 wt %)	−430	0.79	205
Rh (2.1 ± 0.1 wt %)	−168	3.43	99.9

* *Idem* Table 2.

of copper present on the surface after aluminium leaching (Table 3). For deposit, with 10 and 15 wt % Cu–Al, a larger specific surface area was noticed after leaching of aluminium.

The HER Tafel parameters and related overpotentials at 0.1 $A\,cm^{-2}$ are summarized in Table 4 for electrodes made with a graphite powder containing platinum deposits or mixed with a platinum powder. As anticipated, a relationship is noticed between η_{100} and the amount of deposited platinum. In view of the fact that η_{100} is higher for a mixture of pure graphite and platinum powders with 1 : 1 wt than for a graphite powder with only 5.4 wt % deposited platinum, it is deduced that a very fine dispersion of platinum on a graphite surface allows the optimized use of this metal for the HER.

In another set of experiments, Au, Pd and Rh were deposited on a graphite powder and Au/C, Pd/C and Rh/C electrodes were characterized for the HER (Table 5). Of the three electrode materials referred to Table 5, the Rh/C facilitates the HER. As far as Pd/C electrodes are concerned, Pd was difficult to evaporate by resistance heating but an improvement in the HER electrocatalytic activity was noticed for amounts of Pd as low as 0.2 wt %, that is, $\eta_{100} = -430$ mV for Pd/C compared to −525 mV for pure graphite.

3.3. *A.c. measurements*

Pd/C, Pt/C (2.5 wt %) and Rh/C electrodes were characterized for the HER in 1 M KOH solution using an a.c. impedance technique. Rh/C and Pt/C are the best electrocatalytic materials for the HER among the electrode materials investigated in the present paper while Pd/C proved poor by comparison. The frequency of the a.c. current was varied from 0.005 to 20 kHz.

Impedance spectra for the three electrodes under consideration follow a semicircular curve (Figs 7–9). The impedance data were analyzed assuming that the equivalent circuit comprised of the solution resistance R_s in series with the double-layer capacitance, C_{dl}, which in turn is in parallel to the faradaic impe-

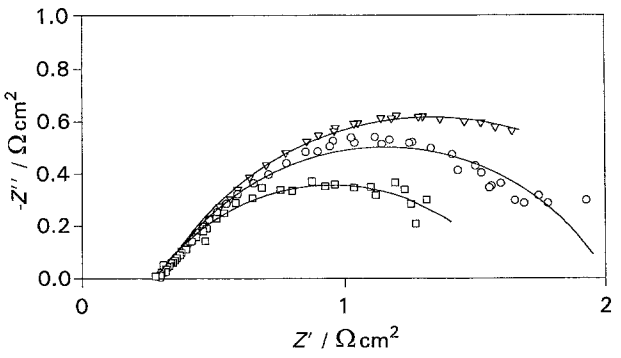

Fig. 7. Nyquist plots for the hydrogen evolution reaction of the Rh/C/$LaPO_4$ electrode in a 1 M solution of KOH at 25 °C. Points are experimental data obtained for various overvoltages: $\eta = -26$ mV (▽), −60 mV (○) and −133 mV (□); lines are calculated.

dance Z_f. According to Harrington and Conway [29], the faradaic admittance ($\hat{Y}_f$) of the system, described by Reactions 1–3, can be represented by the equation

$$\hat{Y}_f = \frac{1}{\hat{Z}_f} = A + \frac{B}{j\omega + C} \tag{9}$$

where

$$A = -F\left(\frac{\partial r_0}{\partial \eta}\right)_\theta \tag{10}$$

$$B = -\frac{F^2}{\sigma_1}\left(\frac{\partial r_0}{\partial \theta}\right)_\eta \left(\frac{\partial r_1}{\partial \eta}\right)_\theta \tag{11}$$

$$C = -\frac{F}{\sigma_1}\left(\frac{\partial r_1}{\partial \theta}\right)_\eta \tag{12}$$

and

$$r_0 = v_1 + v_2 \tag{13}$$

$$r_1 = v_1 - v_2 - 2v_3 \tag{14}$$

The structure of metallic deposits on graphite is usually in the form of microcrystals or clusters [30]. For dispersed palladium, the possibility of hydrogen absorption by metal microcrystals should be taken into account [31, 32]. Therefore, along with Reactions 1–3, consideration should also be given to two additional reactions, namely absorption of hydrogen

$$MH_{ads} = MH_{abs} \qquad v_4, k_4, k_{-4} \tag{15}$$

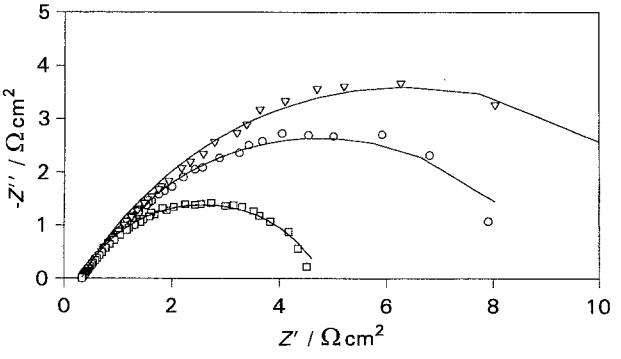

Fig. 8. Nyquist plots for the hydrogen evolution reaction of the Pt/C/$LaPO_4$ electrode in 1 M solution of KOH at 25 °C. Points are experimental data obtained for various overvoltages: $\eta = -189$ mV (▽), −208 mV (○) and −245 mV (□); lines are calculated.

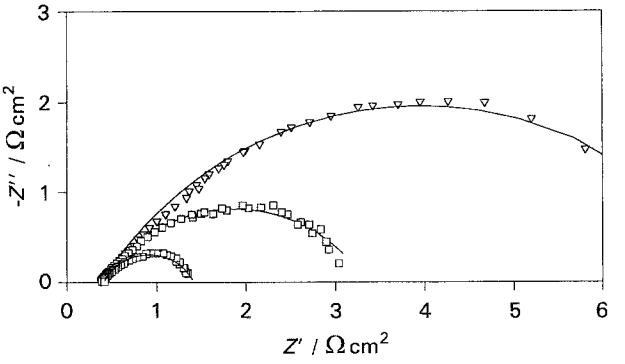

Fig. 9. Nyquist plots for the hydrogen evolution reaction of the Pd/C/$LaPO_4$ electrodes in a 1 M solution of KOH at 25 °C. Points are experimental data obtained for various overvoltages: $\eta = -270$ mV (▽), −360 mV (○) and −443 mV (□); lines are calculated.

and a recombination of absorbed hydrogen

$$2MH_{abs} = H_2 + 2M \qquad v_5, k_5 \tag{16}$$

The reaction rates may be described by

$$v_4 = k_4\theta - k_{-4}X \tag{17}$$

$$v_5 = k_5X^2 \tag{18}$$

where X is the tridimensional occupation coefficient. Under steady-state conditions

$$\frac{\sigma_1}{F}\frac{d\theta}{dt} = r_1 = v_1 - v_2 - v_4 = 0 \tag{19}$$

$$\frac{\sigma_x}{F}\frac{dX}{dt} = r_2 = v_4 - 2v_5 = 0 \tag{20}$$

where σ_x is the charge corresponding to maximum tridimensional absorption of hydrogen. From Equations 17, 18 and 20, X can be expressed as

$$X = \frac{-k_{-4} + \sqrt{(k_{-4}^2 + 8k_4k_5\theta)}}{4k_5} \tag{21}$$

and from Equations 13, 17 and 19

$$\theta = \frac{k_1 e^{-\alpha_1 f\eta} + k_{-2}e^{(1-\alpha_2)f\eta} + k_{-4}X}{k_1 e^{-\alpha_1 f\eta} + k_{-1}e^{(1-\alpha_1)f\eta} + k_2 e^{-\alpha_2 f\eta} + k_{-2}e^{(1-\alpha_2)f\eta} + k_4} \tag{22}$$

In the absence of the absorption reaction ($k_4 = k_{-4} = 0$), Equation 21 is simplified to the form developed earlier [33].

To find an equation describing the faradaic admittance, a Taylor series expansion should be solved for the current, Δi, Δr_1 and Δr_2

$$\Delta i = f\left[\left(\frac{\partial r_0}{\partial \eta}\right)_\theta \Delta\eta + \left(\frac{\partial r_0}{\partial \theta}\right)_\eta \Delta\theta\right] \tag{23}$$

$$\Delta r_1 = \left(\frac{\partial r_1}{\partial \eta}\right)_{\theta,X}\Delta\eta + \left(\frac{\partial r_1}{\partial \theta}\right)_{\eta,X}\Delta\theta + \left(\frac{\partial r_1}{\partial X}\right)_{\eta,\theta}\Delta X \tag{24}$$

$$\Delta r_2 = \left(\frac{\partial r_2}{\partial \theta}\right)_X \Delta\theta + \left(\frac{\partial r_2}{\partial X}\right)_\theta \Delta X \tag{25}$$

where the symbol Δ of the parameter p is described as $\Delta p = pe^{j\omega t}$ and other parameters have their usual meaning.

The following equations are derived from Equations 19, 20, 24 and 25:

$$\tilde{\theta} = \frac{F}{\sigma_1} \frac{\left(\frac{\partial r_1}{\partial \eta}\right)_{\theta,X} \tilde{\eta} + \left(\frac{\partial r_1}{\partial X}\right)_{\eta,\theta} \tilde{X}}{j\omega - \frac{F}{\sigma_1}\left(\frac{\partial r_1}{\partial \theta}\right)_{\eta,X}} \quad (26)$$

$$\tilde{X} = \frac{F}{\sigma_X} \frac{\left(\frac{\partial r_2}{\partial \theta}\right)_X \tilde{\theta}}{j\omega - \frac{F}{\sigma_X}\left(\frac{\partial r_2}{\partial X}\right)_\theta} \quad (27)$$

$$\tilde{i} = F\left[\left(\frac{\partial r_0}{\partial \eta}\right)_\theta \tilde{\eta} + \left(\frac{\partial r_0}{\partial \theta}\right)_\eta \tilde{\theta}\right] \quad (28)$$

The faradaic admittance is equal to

$$\tilde{Y}_f = \tilde{i}/\tilde{\eta} \quad (29)$$

From the above considerations, the faradaic admittance of the system is theoretically characterized by three time constants. It should be noted that the systems studied in the present investigation were characterized by a single time constant, since just one semicircle was observed on the Nyquist plots (Figs 7–9). Thus, for the frequency range under consideration, Reactions 15 and 16 cannot apply so that Equations 9–13 (simplified) may be used. However, the steady-state surface and bulk coverage parameters for hydrogen adsorption may be different from those obtaining in the absence of absorption. In the considerations presented below, the influence of hydrogen absorption has been neglected. For all electrodes investigated, the results could be described assuming a simpler model where the faradaic impedance equals the charge-transfer resistance ($R_{ct} = 1/A$).

In all the cases, the model of Brug *et al.* [34] for the electrode process occurring on solid electrodes was used. According to this model, the total impedance Z_f may be written

$$\hat{Z} = R_s + \frac{1}{\hat{Y}_{el}} \quad (30)$$

where the electrode admittance $\hat{Y}_{el}$ is described by

$$\hat{Y}_{el} = Y_f + (i\omega)^\varphi T = A + \frac{B}{j\omega + C} + (i\omega)^\varphi T \quad (31)$$

and the parameter T is related to the average capacitance per true microscopic surface area (C_{dl}):

$$T = C_{dl}^\varphi (R_s^{-1} + A)^{1-\varphi} \quad (32)$$

This model predicts a rotation of a semicircle with respect to the real axis by the angle φ.

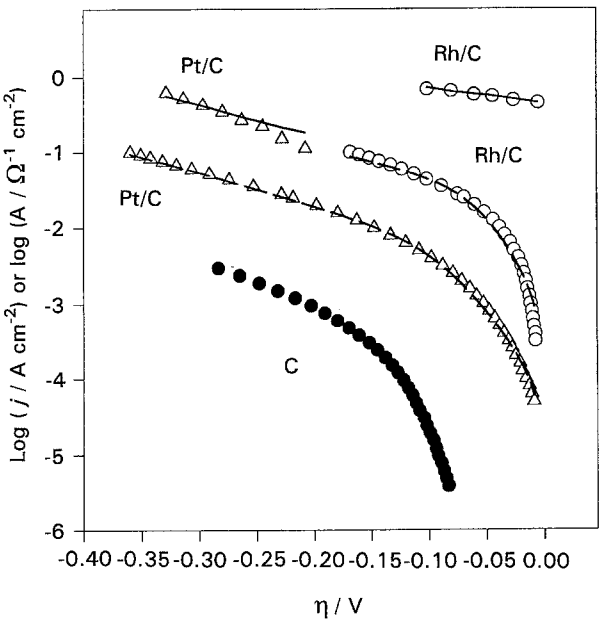

Fig. 10. Dependence of $\log j$ (in A cm^{-2}) and $\log A$ (in Ω^{-1} cm^{-2}) against overpotential for Rh/C and Pt/C electrodes in 1 M KOH at 25 °C; symbols–experimental, lines–calculated (continuous lines: $\log A$, dashed lines: $\log i$): (●) graphite, (△) Pt/C, (○) Rh/C.

The experimental data were fitted to the model described by Equation 30 using different statistical weights. Calculations were performed using a modified complex nonlinear least squares (CNLS) fitting program written by Macdonald [35]. It was found that the best fit between the data and calculated values was obtained for weights proportional to the calculated functions, as suggested by Macdonald. The choice of the model and other weighting modes was described earlier [36].

The parameters $\log A$ and $\log j$ are plotted against the HER overvoltage for Rh/C and Pt/C electrodes in Fig. 10 which also gives the $\log j$ against η curve for a carbon electrode free of deposited metal.

The data of Fig. 10 were analyzed to determine the electrode process. The first step was to consider the Volmer–Heyrovsky (V–H) mechanism. Further, the parameters j, A, T and θ were then determined by envisaging the Volmer–Heyrovsky–Tafel (V–H–T) and Volmer–Tafel (V–T) pathways. The standard deviation of the fit (σ^2) and the average relative standard deviation of the parameters (PD_{av}) as defined by

$$PD_{av} = \frac{1}{N}\sum_k^N \sigma_k \quad (33)$$

where σ_k is the standard deviation of parameter k and N the number of adjustable parameters, were used to

Table 6. Rate constants for the HER on Rh/C, Pt/C and Pd/C electrodes

Electrode materials	k_1 /M cm^{-2} s^{-1}	k_{-1} /M cm^{-2} s^{-1}	k_2 /M cm^{-2} s^{-1}	α_1	α_2
Rh/C (2.1 ± 0.1) wt %	$1.9 \pm 0.3 \times 10^{-4}$	$6.2 \pm 0.5 \times 10^{-9}$	$1.1 \pm 0.1 \times 10^{-7}$	0.5	0.22 ± 0.03
Pt/C (2.5 ± 0.1) wt %	$1.1 \pm 0.1 \times 10^{-8}$	$4.1 \pm 0.1 \times 10^{-10}$	$3.2 \pm 1.3 \times 10^{-7}$	0.31 ± 0.01	0.5
Pd/C (0.2 ± 0.1) wt %	$8.6 \pm 0.4 \times 10^{-9}$	$4.0 \pm 0.3 \times 10^{-11}$	$1.7 \pm 2.1 \times 10^{-8}$	0.23 ± 0.01	0.3

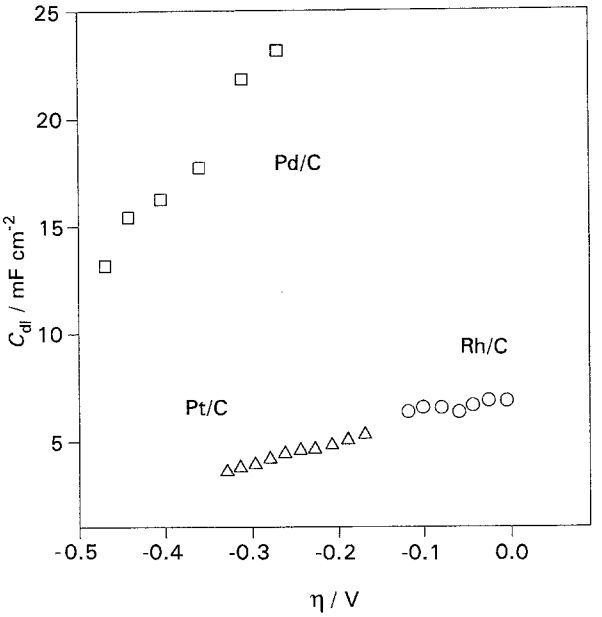

Fig. 11. Dependence of the double-layer capacitance of the Pd/C, Pt/C and Rh/C electrodes on overvoltage in 1 M KOH at 25 °C.

distinguish the mechanism for which the best fits of the experimental data are obtained. For Rh/C, Pt/C and Pd/C electrodes, the best fits were obtained with the Volmer–Heyrovsky mechanism; the corresponding kinetic parameters are summarized in Table 6. The rate constant k_1 obtained for the Rh/C electrodes is almost 3000 times higher than k_1 for the rhodium powder electrode [36]. The limiting rate constant of the HER decreases from $\sim 10^{-7}$ M cm^{-2} s^{-1} for Rh/C to $\sim 10^{-9}$ M cm^{-2} s^{-1} for Pd/C electrodes which is in agreement with the electrocatalytic activity deduced from Tafel curves (Tables 4, 5).

In Fig. 11, the double-layer capacitance is expressed versus the hydrogen overvoltage for Rh/C, Pt/C and Pd/C electrodes and the highest C_{dl} values noticed, at any overpotential, are for Pd/C electrodes. Assuming the capacitance of the graphite electrode is

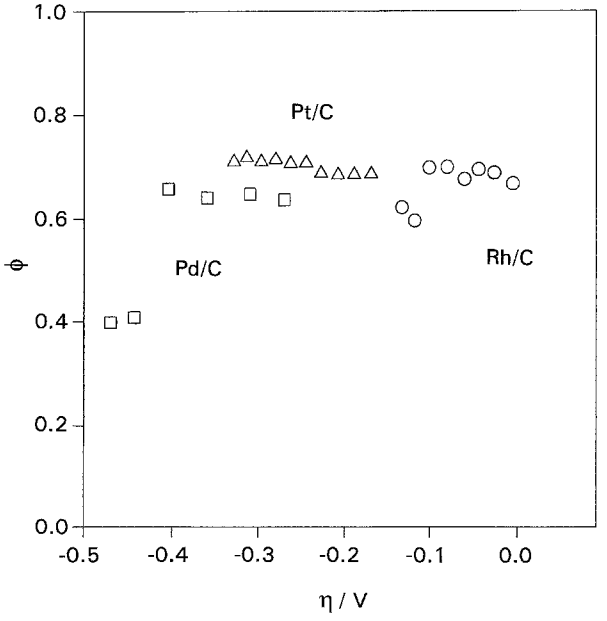

Fig. 12. Dependence of ϕ determined for Pt/C, Pd/C and Rh/C electrodes on overvoltage in 1 M KOH at 25 °C.

$\sim 20\ \mu$F cm^{-2} [37], the estimated surface roughness factor is ~ 250 for Pt/C and Rh/C electrodes but varies from ~ 650 to ~ 1200 for Pd/C electrodes. The dependence of the angle ϕ on η (Fig. 12) suggests a higher porosity for the Pd/C electrodes. Although the relationship between the fractal dimension (D) and ϕ is still controversial [38, 39], a lower ϕ is generally postulated for a larger surface roughness factor. For Pd/C electrodes, the low electrocatalytic activity noticed despite the high roughness factor is possibly induced by the high solubility of hydrogen in palladium microcrystals [31].

4. Conclusions

A new method of obtaining highly dispersed electrocatalytic materials has been successfully developed by vacuum deposition of catalytic metals on electromechanically suspended graphite powder. Structural investigation provides evidence of the uniform dispersion of metal on graphite particle surfaces. Electrodes with good mechanical strength and chemical stability are obtained by binding powder particles with an inorganic polymer of $LaPO_4$. In 1 M KOH solution at 25 °C, the electrocatalytic activity for the HER is improved by the presence of a metal (or alloy) on pure graphite particles. For the Rh/C (2.1 wt %), Pt/C (2.5 wt %) and Pd/C (0.2 wt %) electrodes, a.c. measurements show that the HER proceeds via the Volmer–Heyrovsky mechanism, and Rh/C (2.1 wt %) electrodes having the highest electrocatalytic activity.

Acknowledgements

Special thanks are due to Eric Arsenaud, Marie-Chantal Denis, Stephane Morasse and Pierre Magny from Sherbrooke University for their technical assistance. The financial support of NSERCC is also gratefully acknowledged.

References

[1] M. Enyo, *in* 'Comprehensive treatise of electrochemisty', vol. 7, (edited by B. E. Conway, J. O'M. Bockris, E. Yeager, S. V. M. Khan and R. E. White), Plenum Press, New York (1988) p. 241.
[2] B. E. Conway, *Sci. Progr. Oxford* **71** (1987) 479.
[3] J. O'M. Bockris, *in* 'Comprehensive treatise of electrochemistry', vol. 3, *op cit.* [1], (1981), pp. 1–505.
[4] H. Wendt and G. Imarisio, *J. Appl. Electrochem.* **18** (1988) 1.
[5] J. Divisek, *J. Electroanal. Chem.* **214** (1986) 615.
[6] A. J. Appleby, H. Kita, M. Chemla and G. Bronoël, 'Encyclopedia of electrochemistry of the elements, vol. IXB, (edited by A. J. Bard), Dekker, New York, p. 383; H. Kita *J. Electrochem. Soc.* **113** (1966) 1095.
[7] H. Wendt (ed.), 'Electrochemical hydrogen technologies'. Electrochemical production and combustion of hydrogen, Elsevier, Amsterdam and Tokyo (1990).
[8] G. T. Bowen, H. J. Davis, B. F. Henshaw, R. Lachance, R. L. Leroy and R. Renaud, *Int. J. Hydrogen Energy* **9** (1984) 59.
[9] K. Lohrberg and P. Kohl. *Electrochim. Acta* **29** (1984) 1557.
[10] B.V. Tilak, A.C. Ramamurthy and B.E. Conway, *Proc. Indian. Surf. Sci.*, (Chem. Sci.) **97** (1986) 359.
[11] E. Endoh, H. Otouma, T. Morimoto and Y. Oda, *Int. J. Hydrogen Energy* **12** (1987) 473.

[12] B. E. Conway and L. Bai, *ibid.* **1** (1986) 533.
[13] B. E. Conway, H. Angerstein-Kozlowska and M. A. Sattar, *J. Electrochem. Soc.* **130** (1983) 1825.
[14] D. E. Brown, M. N. Mahmood, M. C. M. Man and A. K. Turner, *Electrochim. Acta* **29** (1984) 1551.
[15] D. E. Hall, *J. Appl. Electrochem.* **14** (1984) 107.
[16] *Idem, J. Electrochem. Soc.* **124** (1981) 740.
[17] E. Potvin, H. Ménard, J.-M. Lalancette and L. Brossard, *J. Appl. Electrochem.* **20** (1990) 252.
[18] J.-M. Lalancette, H. Ménard and E. Potvin, *US Patent 4 886 591* (1989).
[19] E. Potvin, H. Ménard, L. Brossard and J.-M. Lalancette, *Int. J. Hydrogen Energy* **15** (1990) 843.
[20] H. Dumont, P. K. Wrona, L. Brossard, J.-M. Lalancette and H. Ménard, *J. Appl. Electrochem* **22** (1992) 1049.
[21] H. Menard, J. Fournier, L. Brossard, J.-M. Lalancette, *US Patent 2 130 870* submitted.
[22] R. N. Adams, 'Electrochemistry at solid electrodes', Dekker, New York (1969).
[23] J. Fournier, P. K. Wrona, A. Lasia, R. Lacasse, J.-M. Lalancette, H. Menard and L. Brossard, *J. Electrochem. Soc.* **13** (1992) 2372.
[24] H. Dumont, PhD. thesis, Université de Sherbrooke, Sherbrooke, Québec, Canada (1994).
[25] M. Caron, *Geol. Surv. Bull.* (US) **1036** (1958) 253.
[26] D. F. Mullica, W. O. Milligan, D. A. Grossie, G. W. Beall, L. A. Bootner, *Inorganica Chemica Acta* **95** (1984) 231.
[27] L. Holland, 'Vacuum deposition of thin films', Chapman & Hall, London (1970).
[28] S. Dushman, 'Scientific foundations of vacuum technique', J. M. Lafferty, Editor, New York and London (1962).
[29] D. A. Harrington and B. E. Conway, *Electrochim. Acta* **32** (1987) 1703.
[30] J. Chevallier, *Thin Solid Films* **40** (1977) 223.
[31] M. Baldauf and D. M. Kolb, *Electrochimi. Acta* **38** (1993) 2145.
[32] B. E. Conway and G. Jerkiewicz, *J. Electroanal. Chem.* **357** (1993) 47.
[33] A. Lasia and A. Rami, *ibid.* **294** (1990) 123.
[34] G. J. Brug, A. L. G. van der Eeden, M. Sluyters-Rehbach, and J. Sluyters, *ibid.* **176** (1984) 275.
[35] J. R. Macdonald (ed.), 'Impedance spectroscopy', Wiley & Sons, New York (1987).
[36] P. K. Wrona, A. Lasia, H. Ménard and M. Lessard, *Electrochim. Acta* **37** (1990) 1283.
[37] R. L. Brodd and N. Hackerman, *J. Electrochem. Soc.* **104** (1957) 704.
[38] M. Keddam and H. Takenouti, *Electrochim Acta* **33** (1988) 445.
[39] T. Pajkossy, *J. Electroanal. Chem.* **300** (1991) 1.